Highly Active Nitrogen–Doped Carbon Nanotubes for Oxygen Reduction Reaction in Fuel Cell Applications

ARTICLE *in* THE JOURNAL OF PHYSICAL CHEMISTRY C · DECEMBER 2009

Impact Factor: 4.77 · DOI: 10.1021/jp908067v

5 AUTHORS, INCLUDING:

Zhu Chen
Chengdu University of Information Techno…
22 PUBLICATIONS **790** CITATIONS
SEE PROFILE

Drew C Higgins
University of Waterloo
70 PUBLICATIONS **2,082** CITATIONS
SEE PROFILE

Zhongwei Chen
University of Waterloo
179 PUBLICATIONS **5,220** CITATIONS
SEE PROFILE

Highly Active Nitrogen-Doped Carbon Nanotubes for Oxygen Reduction Reaction in Fuel Cell Applications

Zhu Chen, Drew Higgins, Haisheng Tao, Ryan S. Hsu, and Zhongwei Chen*

Department of Chemical Engineering, Waterloo Institute for Nanotechnology, Waterloo Institute for Sustainable Energy, University of Waterloo, Waterloo, Ontario, Canada N2L 3G1

Received: August 20, 2009; Revised Manuscript Received: September 27, 2009

One of the main challenges in the commercialization of low temperature fuel cells is the slow oxygen reduction reaction (ORR) kinetics and the high cost and scarcity of platinum (Pt)-based catalysts. As a result, alternative non-noble electrocatalysts to Pt materials for ORR is needed to realize the practical application of fuel cells. In this study, nitrogen-doped carbon nanotubes (NCNTs) were synthesized as a non-noble electrocatalyst for the ORR using ethylenediamine (EDA-NCNT) and pyridine (Py-NCNT) as different nitrogen precursors by a single-step chemical vapor deposition (CVD) process. The resulting EDA-NCNT has shown similar ORR performance compared to platinum on carbon support in terms of onset and half-wave potentials. Moreover, EDA-NCNT showed superior ORR performance in terms of limiting current density, number of electrons transferred, and H_2O selectivity. The effects of nitrogen content on ORR performance of NCNT were investigated by comparing EDA-NCNT with Py-NCNT. The ORR performance of Py-NCNT was inferior compared to EDA-NCNT in terms of onset and half-wave potentials, limiting current density, number of electrons transferred, and H_2O selectivity. Further material characterizations by X-ray photoelectron spectroscopy (XPS) and Raman spectroscopy illustrated a higher nitrogen content and more defects in EDA-NCNT compared to that of Py-NCNT which indicates the important role of the nitrogen precursor on nitrogen content and structure of NCNT. By combining the results of ORR activity and material characterization, it is concluded that higher nitrogen content and more defects of NCNT lead to high ORR performance.

Introduction

Fuel cells (FCs) have been receiving lots of attention as a sustainable power source for transport, stationary, and portable applications because of their high efficiency and low emissions.[1−4] The slow kinetics of the oxygen reduction reaction (ORR) at the cathode is one of the key factors limiting the performance of low temperature FCs. This is true regardless of the fuel, whether the FC is combusting hydrogen or an alcohol, such as methanol or ethanol.[5] To date, the best materials for the catalysis of the ORR are platinum based; however, they suffer from slow reduction kinetics and high cost, which hinders the large-scale commercialization of low temperature FCs. As a result, inexpensive, highly active, and durable ORR electrocatalysts will accelerate the process of commercialization of FCs. Tremendous efforts have been made toward the development of non-noble metal catalysts in the last several decades. Different types of non-noble catalysts, such as transition metal alloys[6] and chalcogenides,[7] have been explored in recent years. These catalysts have shown promising activity for application in FCs, but their performance is inferior compared to that of Pt catalysts.

The newly emerging field of nanotechnology has the potential to make a significant impact on the electrocatalysts for the ORR by introducing novel nanoscale materials.[8] Carbon nanotubes (CNT) have been utilized as catalyst supports to reduce Pt loading and improve long-term stability.[9−11] By doping CNTs with nitrogen, the ORR activity of the resulting nitrogen-doped carbon nanotubes (NCNT) was improved significantly.[12] Although the ORR activity of CNT was greatly improved through nitrogen doping, the ORR activity is poor compared to platinum based materials.[13,14] Recently, Gong et al. successfully synthesized NCNT that show better electrocatalytic activity and long-term stability compared to platinum on carbon support (Pt/C) in alkaline conditions.[15] It has been demonstrated that nitrogen on the surface of the carbon was an essential requirement to obtain non-noble metallic-based catalytic sites, however, their ORR mechanism is poorly understood. It has been proposed that the catalytic activity observed on NCNT may be attributed to two different active sites. Specifically, one relates the origin of the ORR activity in NCNT with the transition metal−nitrogen groups (FeN_4), similar to those found in transition-metal macrocycles.[16,17] The other attributes the source of the ORR activity in NCNT to surface nitrogen in the form of pyridinic and pyrrolic/pyridone-type nitrogen groups.[14,18] Since both views emphasize the presence of nitrogen in the active site, nitrogen content in NCNT is expected to be a governing factor with respect to the ORR activity. Thus, using different nitrogen precursors for NCNT synthesis could lead to varying nitrogen content, which is hypothesized to affect the ORR activity of the resultant NCNT.

This paper presents the synthesis of NCNT using ethylenediamine (EDA) and pyridine (Py) as different nitrogen precursors, and ferrocene (Fc) as a catalyst through a single-step chemical vapor deposition (CVD) process. The NCNT grown from the Fc/EDA mixture (EDA-NCNT) will be used for the first time as a non-noble ORR catalyst. The difference in the ORR activity between EDA-NCNT and NCNT grown from Fc/Py mixture (Py-NCNT) will be discussed. Furthermore, the effect of different nitrogen precursors on the nitrogen content and the ORR electrocatalytic activity of NCNT will be investigated by comparing EDA-NCNT and Py-NCNT.

* To whom correspondence should be addressed. E-mail: zhwchen@uwaterloo.ca.

10.1021/jp908067v CCC: $40.75
Published on Web 11/13/2009

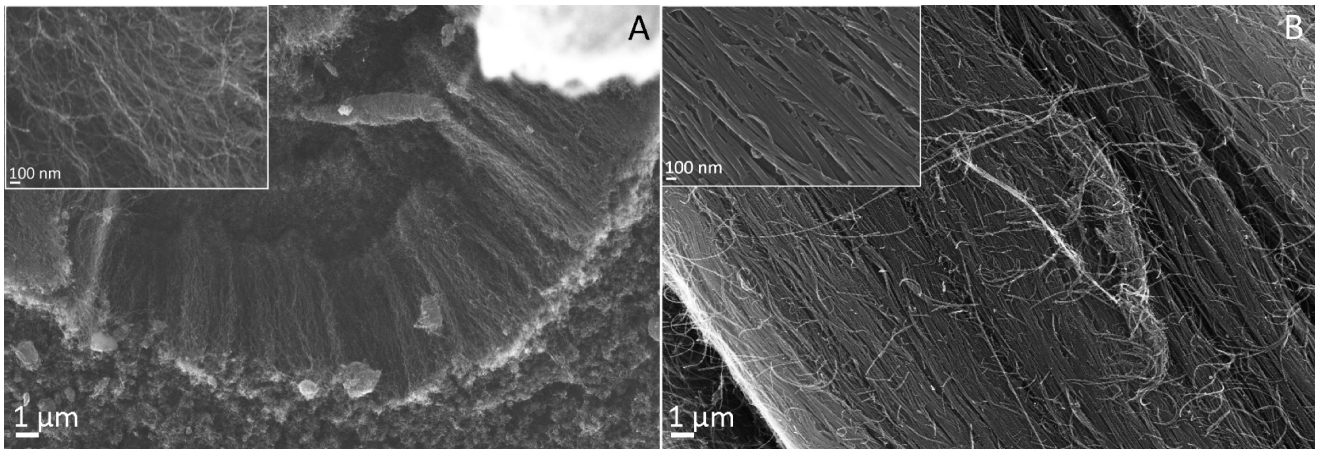

Figure 1. SEM image of (A) EDA-NCNT and (B) Py-NCNT. The alignment of the NCNT is better in Py-NCNT compared to EDA-NCNT.

Experimental Methods

NCNT synthesis: NCNT were grown by an injection CVD method, where ferrocene (98%, Aldrich) was used as a catalyst and pyridine (99% Caledon Laboratory Chemicals) or ethylenediamine (98% EMD Chemicals) was used as a carbon and nitrogen precursor. Quartz tubes (O.D 18 mm, length 100 mm) and silicon wafers (~1 cm × 1 cm) were used as the substrates for NCNT growth for the injection CVD method. Ferrocene was dissolved in the precursors mentioned above at 2.5 wt %. Silicon wafer substrates were placed in the middle of the quartz tube, which was loaded into the center of an alumina tube (1″ outer diameter) surrounded by a single zone furnace system. The carrier gas used was argon, and the reaction was carried out at 800 °C for 1 h under ambient pressure. The NCNT were obtained from the soot deposited on the surface of the quartz tube after growth. The obtained products were subjected to acid treatment by boiling in 0.5 M sulfuric acid for 5 h and were dried at 70 °C in a vacuum oven overnight.

Characterization: Scanning electron microscopy (LEO FESEM 1530, 20 eV) was used to investigate the overall morphology of NCNT. Transmission electron microscopy (Philips CM300) was used to examine the graphitization of the NCNT walls and to observe defect sites. X-ray photoelectron spectroscopy (Thermal Scientific K-Alpha XPS spectrometer, 150 eV) was used to investigate the relative content of different elements and the intensity of different nitrogen groups in the NCNT. Energy dispersive X-ray spectroscopy was used to evaluate the elemental composition of the NCNT samples.

Electrocatalytic activity evaluation: Electrocatalytic activity was evaluated using rotating ring disk electrode voltammetry. The instruments used include a biopotentiostat and a rotation speed controller (Pine Research Instrumentation). The RRDE experiment was carried out under alkaline conditions using 0.1 M potassium hydroxide as an electrolyte and an Ag/AgCl reference electrode. The potential was varied from 0.2 to −1.2 V vs Ag/AgCl (figures only to −0.5 V) at the potential sweep rate of 10 mV/s, and the ring potential was set at 0.5 V. The ink for RRDE consists of 2 mg of NCNT suspended in 2 mL of 0.2 wt % Nafion solution. For each RRDE experiment, 20 μL of NCNT ink was deposited onto the glassy carbon electrode. Before each experiment, nitrogen gas was saturated in the electrolyte by bubbling the gas for 30 min. The results of experiments with nitrogen gas were used as a background. After a background scan was performed, oxygen gas was introduced to the system by bubbling for 30 min to saturate the solution and then a RRDE experiment was performed.

TABLE 1: Summary of the Elemental Compositions of EDA-NCNT and Py-NCNT after Acid Leaching from EDX

composition	EDA-NCNT (at. %)	Py-NCNT (at. %)
carbon	84.48	89.65
nitrogen	5.58	3.41
oxygen	8.33	5.18
iron	1.61	1.77

Results and Discussion

The morphology of EDA-NCNT and Py-NCNT was investigated by scanning electron microscopy (SEM). Nanotube alignment was observed for both EDA-NCNT (Figure 1A) and Py-NCNT (Figure 1B). Along the nanotube growth axis, a zigzag pattern was observed for EDA-NCNT (Figure 1A inset), whereas a relatively more straight geometry was observed for Py-NCNT (Figure 1B inset). Energy dispersive X-ray spectroscopy (EDX) was performed simultaneously with SEM imaging. EDX analysis showed that the atomic composition from highest to lowest in the EDA-NCNT and Py-NCNT was carbon, oxygen, nitrogen, and iron. These results and their respective compositions can be found in Table 1. This shows that nitrogen was successfully incorporated into both catalyst samples. A more detailed study on the nitrogen content and its bonding with the native carbon atoms by X-ray photoelectron spectroscopy (XPS) will be presented later in this paper. The presence of oxygen was observed in both samples, which could be attributed to the fact that air was allowed to enter the furnace at 400 °C for the purpose of burning off amorphous carbon after the growth was completed.

The NCNT formed were observed using transmission electron microscopy (TEM) which show bamboo-like structures for EDA-NCNT (Figure 2A) and Py-NCNT (Figure 2B), a common feature of NCNT published in many reports.[19−22] The formation of the bamboo-like structure is attributed to the more energetically favorable formation of a positive curvature surface during the substitution of nitrogen atoms into the graphitic structure.[23] More rounded compartments were observed for EDA-NCNT, whereas Py-NCNT demonstrated more rectangular compartments. Apart from the difference in compartments, the graphitic walls of the nitrogen rich EDA-NCNT are thinner compared to the relatively nitrogen deficient Py-NCNT which correlates to the increase in overall nitrogen content.[19,20]

Rotating ring disk electrode (RRDE) voltammetry was used to evaluate the electrocatalytic activity of NCNT in the ORR (Figure 3). The half-wave potential (HWP), limiting current density, number of electrons transferred in reaction, and H_2O

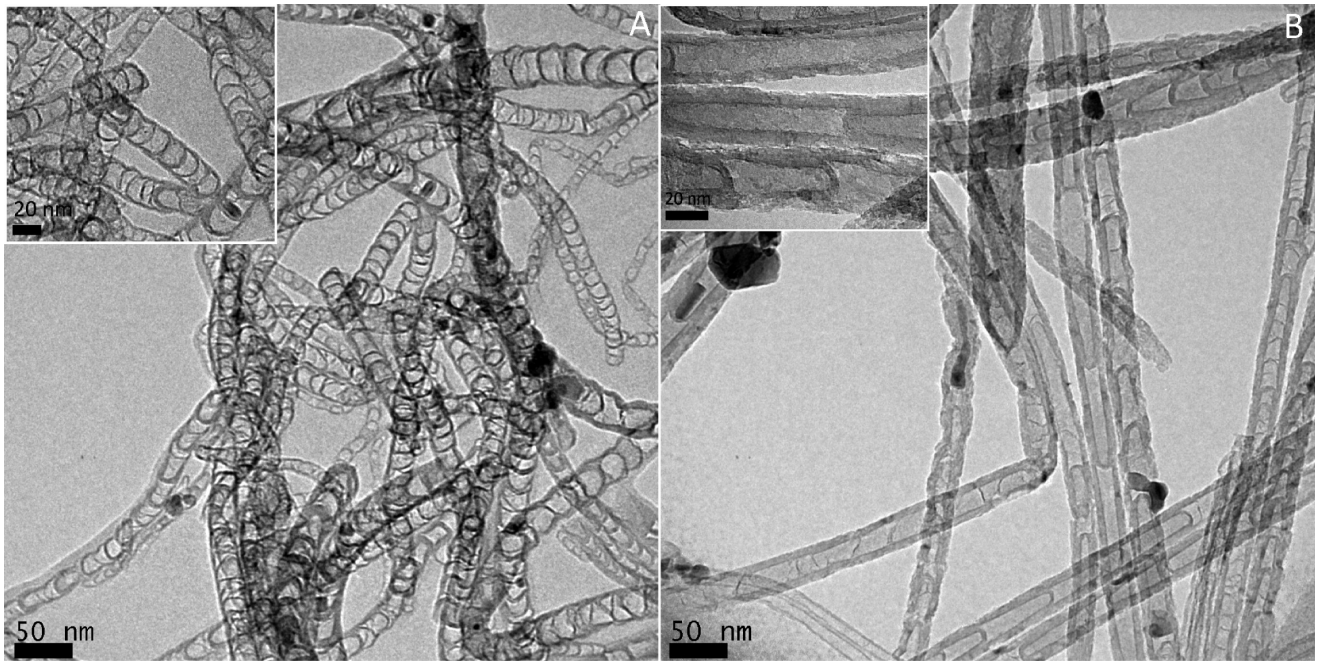

Figure 2. TEM image of (A) EDA-NCNT and (B) Py-NCNT. The bamboo structure is shown in both images. The scale bar in the inset of A and B is 20 nm.

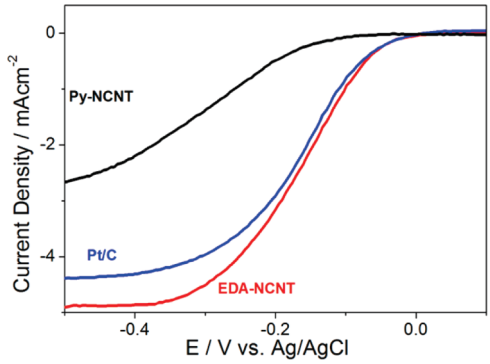

Figure 3. Polarization curve of EDA-NCNT, Py-NCNT, and Pt/C at 1600 rpm. EDA-NCNT shows better ORR catalytic performance compared to Py-NCNT and Pt/C.

TABLE 2: Summary of the Important Performance Indicators of ORR Catalysis[a]

	half wave potential (V)	limiting current density (mA cm^{-2})	number of electron transferred (at 1600 rpm)		H_2O selectivity (%) (at 1600 rpm)	
EDA-NCNT	−0.15	−4.91	3.63*	3.85‡	84.69*	92.62‡
Py-NCNT	−0.33	−1.57	–	3.42‡	–	71.02‡
Pt/C	−0.16	−4.39	3.55*	3.82‡	81.33*	91.82‡

[a] Starred (*) entries indicate values taken at −0.1 V, and the double daggered entries (‡) indicate values taken at −0.3 V.

selectivity are summarized in Table 2. It is clear that the ORR activity of EDA-NCNT is similar to commercial Pt/C catalyst and superior to Py-NCNT with respect to every parameter investigated (Table 2). Compared to Py-NCNT, a 3-fold increase in limiting current density was observed in EDA-NCNT. In addition, a 0.17 V improvement in HWP is observed for EDA-NCNT (onset potential of 0 V vs Ag/AgCl) compared to that of Py-NCNT (onset potential of −0.2 V vs Ag/AgCl), and the number of electrons transferred was improved by 12.6% at −0.3 V. Similarly, with respect to H_2O selectivity, EDA-NCNT showed a significant 21.6% improvement compared to Py-NCNT. With regard to EDA-NCNT and Pt/C, EDA-NCNT displayed slight improvement in HWP, number of electrons transferred, and H_2O selectivity. However, a 12% increase in limiting current density was observed in EDA-NCNT compared to Pt/C.

The kinetic analysis of the ORR performance of EDA-NCNT, Py-NCNT, and Pt/C can be carried out by the Koutecky−Levich (K-L) equation (Figure 4):

$$\frac{1}{i} = \frac{1}{i_k} + \frac{1}{B\sqrt{\omega}} \quad (1)$$

where i_k is the kinetic current density, B is the Levich slope, ω is the rotation speed, and i is the observed current density. The Levich slope can be further defined as:

$$B = 0.62nFC_{O_2}D_{O_2}^{2/3}V^{1/6} \quad (2)$$

where n is the number of electrons transferred, F is the Faraday constant, C_{O_2} is the bulk oxygen concentration, D_{O_2} is the diffusion coefficient of oxygen, and V is the viscosity of the solution. The K-L relationship is valid in the mixed diffusion and kinetic limited regime. From the K-L plots of EDA-NCNT and Pt/C, similar slopes are an indication of the first-order reaction kinetics of the ORR.[24,25] The slope of the K-L plots of Py-NCNT at different potentials varies greatly, indicating the kinetics of the ORR catalysis by Py-NCNT may differ from the first-order kinetics observed by both Pt/C and EDA-NCNT. From eq 1, values of i_k at different potentials can be obtained by taking the inverse of the Y-intercept in the respective K-L plots. The highest calculated kinetic current density was observed for EDA-NCNT showing a 46% increase compared to Pt/C and 123% increase compared to Py-NCNT (Table 3).

Information regarding the mechanism of O_2 adsorption can be obtained through the Tafel slopes in the generated Tafel plots (Figure 5). The interval used to determine the Tafel slopes in low and high current density regions are from −1.2 to −0.7 and −0.4 to 0.1, respectively, in the log scale. The use of fixed

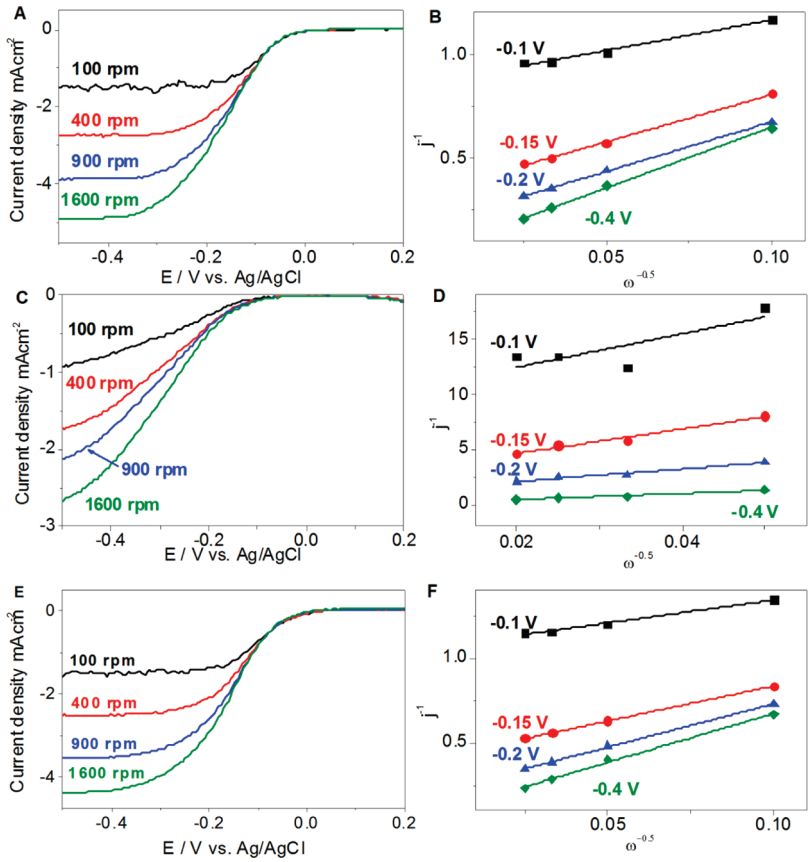

Figure 4. Koutecky−Levich plot of (A) EDA-NCNT, (C) Py-NCNT, and (E) Pt/C at different potential. Polarization curve of (B) EDA-NCNT, (D) Py-NCNT, and (F) Pt/C at different electrode rotation speeds.

TABLE 3: Kinetic Current of EDA-NCNT, Py-NCNT, and Pt/C at Different Potentials

E/V vs Ag/AgCl	EDA-NCNT (i_k/mA cm^{-2})	Pt/C (i_k/mA cm^{-2})	Py-NCNT (i_k/mA cm^{-2})
−0.1	1.15	0.93	0.11
−0.15	2.85	2.37	0.42
−0.2	5.07	4.56	1.11
−0.4	15.06	10.31	6.76

intervals for Tafel slope determination is necessary for a fair comparison between different samples. The Tafel slope in the low and high current density region of the Pt/C sample is −0.06368 V dec^{-1} and 0.11999 V dec^{-1}, respectively (Figure 5D). The presence of two different slopes corresponds to the switch between Langmuir adsorption and Temkin adsorption of oxygen on the Pt/C catalyst. The Tafel plot of EDA-NCNT shows a similar profile with a Tafel slope of −0.06561 V dec^{-1} in the low current density region and −0.11383 V dec^{-1} in the high current density region (Figure 5B), indicating similar adsorption kinetics of EDA-NCNT compared to Pt/C. The Tafel slope of Py-NCNT is −0.09666 V dec^{-1} and −0.25259 V dec^{-1} at low and high current densities respectively (Figure 5C). This large variation of Tafel slope of Py-NCNT indicates much different adsorption kinetics of Py-NCNT compared to EDA-NCNT and Pt/C.

The elemental composition and different structural groups of nitrogen in EDA-NCNT and Py-NCNT was obtained using XPS (Figure 6 and Figure 7). From XPS results, EDA-NCNT showed higher nitrogen content compared to Py-NCNT (Table 4). Higher nitrogen content in EDA-NCNT were expected, as each EDA molecule contains two nitrogen atoms whereas only one nitrogen atom is present in each Py molecule. Consequently,

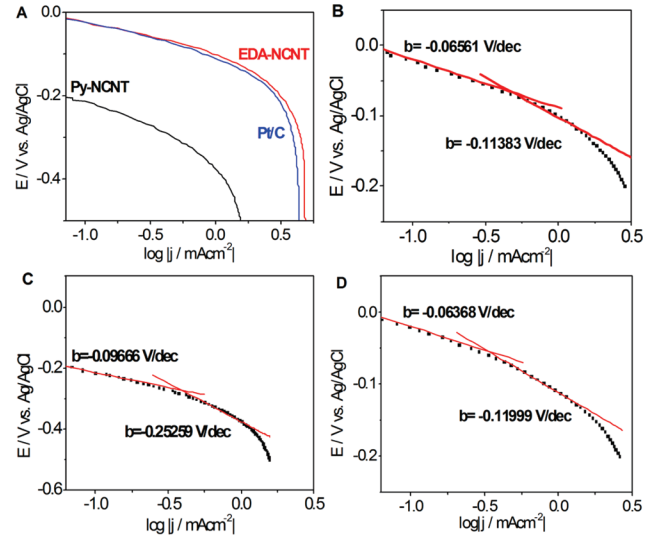

Figure 5. Tafel plot of (A) EDA-NCNT, Py-NCNT, and Pt/C and linear fit to the low and high density regime of (B) EDA-NCNT, (C) Py-NCNT, and (D) Pt/C. The data used in the above plots are at 1600 rpm.

higher nitrogen to carbon ratio in the growth environment was achieved during CNT synthesis when EDA was used. This result agrees with the literature which shows a positive correlation between NCNT nitrogen content and the number of nitrogen atoms in the precursor molecules.[26]

From the analysis of the N 1S signal (Figure 7), peaks centered at 398.47, 400.75, and 404.87 eV were observed for Py-NCNT. Similar peaks centered at 398.60, 401.05, and 404.69 eV were observed for EDA-NCNT. The peaks at around 398.6

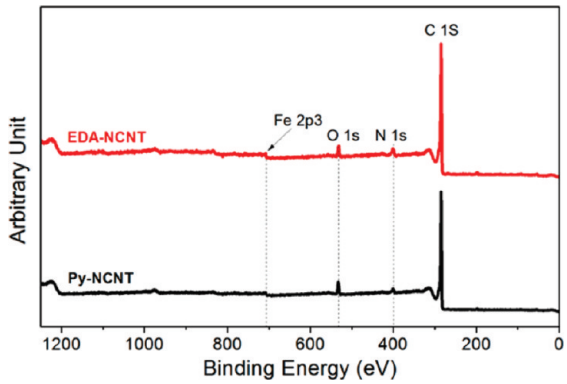

Figure 6. XPS spectrum of EDA-NCNT and Py-NCNT showing all the elements in the samples.

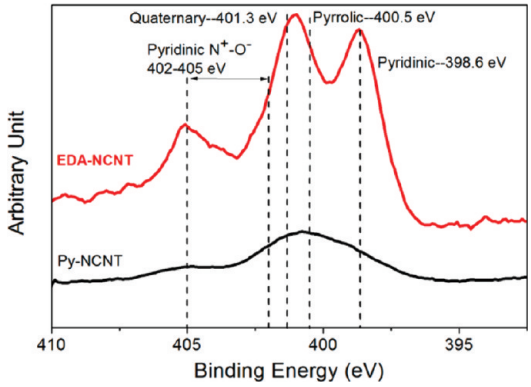

Figure 7. XPS spectrum showing the presence of different types of nitrogen groups from the N 1S signal of EDA-NCNT and Py-NCNT.

TABLE 4: XPS Analysis of the Elemental Composition of EDA-NCNT and Py-NCNT after Acid Leaching

	EDA-NCNT		Py-NCNT	
composition	peak position (eV)	at. %	peak position (eV)	at. %
carbon	284.69	91.50	284.64	92.70
nitrogen	400.84	4.74	399.88	2.35
oxygen	531.65	3.38	532.57	4.75
iron	707.28	0.38	708.01	0.20

and 404.6 eV refer to pyridinic nitrogen and pyridinic N^+-O^- groups, respectively. There is some ambiguity toward the peaks at 401.05 and 400.75 eV from EDA-NCNT and Py-NCNT, respectively, since they are close to the peak of the pyrrolic nitrogen group at 400.5 eV but also close to quaternary nitrogen at 401.3 eV. Hence, it is proposed that the peaks at 401.03 and 400.75 eV indicate the coexistence of quaternary and pyrrolic nitrogen groups. The peak from EDA-NCNT at 401.03 eV is much closer to the quaternary nitrogen peak position (401.3 eV), and the peak of Py-NCNT at 400.75 eV is much closer to the pyrrolic nitrogen peak position (400.5 eV). Therefore, it is concluded that EDA-NCNT contains more quaternary nitrogen whereas Py-NCNT contains more pyrrolic nitrogen. In addition, since the NCNT synthesis was carried out under ambient conditions, the reaction between oxygen and nitrogen during synthesis results in the formation of pyridinic N^+-O^-.

More pyridinic nitrogen groups were observed in EDA-NCNT than seen in Py-NCNT (Table 5), which agrees with the results of other studies where at higher overall nitrogen content, the formation of pyridinic nitrogen is preferred.[19,27] On the contrary, for Py-NCNT containing less overall nitrogen, quaternary nitrogen was the dominant product, similar to results obtained

TABLE 5: Detail Breakdown of N 1S Signal of EDA-NCNT and Py-NCNT after Acid Leaching[a]

	EDA-NCNT		Py-NCNT	
composition	peak position (eV)	at. %	peak position (eV)	at. %
quaternary/pyrrolic	401.05	45.91	400.75	68.20
pyridinic	398.60	35.09	398.47	14.83
pyridinic N^+-O^-	404.69	19.00	404.87	16.96

[a] Quaternary and pyrrolic nitrogen groups both contribute to the peak centered at 401.05 and 400.75 eV in EDA-NCNT and Py-NCNT.

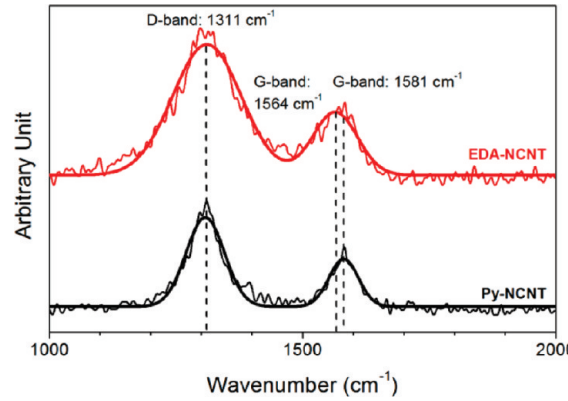

Figure 8. The Raman spectrum of EDA-NCNT and Py-NCNT showing the D- and G-band. The spectra are fitted to two Gaussian-like components. The G-band of EDA-NCNT shows a slight down shift of the G-band and higher intensity of the D-band relative to Py-NCNT.

by Terrones et al.[19,20] In NCNT there is a tendency for substituted nitrogen atoms to form on the inner walls of multiwalled carbon nanotubes.[23] Hence, the amount of quaternary nitrogen on the outermost graphite wall could be lower than the total amount reported from XPS analysis which reduces the amount of quaternary nitrogen available for ORR. Since the nitrogen group on the outermost graphite wall is most important for ORR, it suggests that quaternary nitrogen does not have a big impact on the ORR. From XPS, EDA-NCNT contains a significantly higher pyridinic nitrogen content of 1.7 at.% compared to Py-NCNT at 0.3 at.%. Formation of pyridinic nitrogen groups is often observed on the edge of the graphite plane, and the lone pair of electrons from pyridinic nitrogen groups has been attributed be ORR acitive.[28] The higher exposure of the planar edges of graphite in EDA-NCNT due to the more rugged surface structure is expected to expose more pyridinic nitrogen which enhances the ORR activity. This explains the significant improvement in the ORR activity of EDA-NCNT over Py-NCNT.

Raman spectroscopy was also used to provide information on the degree of structural defect of NCNT (Figure 8). For EDA-NCNT, the peak centered at 1311 cm^{-1} is the Raman active D-band and the other centered at 1564 cm^{-1} is the Raman active G-band. The D- and G-bands are also present in Py-NCNT centered at 1307 cm^{-1} and 1581 cm^{-1}, respectively. The D-band is ascribed to the finite-sized crystals of graphite, which become active because of a reduction in symmetry near or at the crystalline edges.[29] The G-band is due to the E_{2g} vibration mode and is observed in all sp^2 bonds in a graphitic network.[29] The intensity ratio of the D- to G-band (I_D/I_G) gives qualitative information comparison for the degree of defects in NCNT. A higher ratio indicates more defects present in the nanotubes. From Raman spectra, the I_D/I_G ratio of Py-NCNT and EDA-

NCNT is 1.87 and 2.07, respectively, indicating a higher degree of defects in EDA-NCNT which could be caused by the higher nitrogen content. This conclusion is consistent with the TEM images and XPS data. With respect to Py-NCNT, the Raman spectrum of EDA-NCNT showed a slight downshift of the G-band, possibly caused by the change in electronic structure of NCNT due to the higher nitrogen content.[30]

Conclusions

The high ORR activity observed for EDA-NCNT and additional benefits of CNT such as superior mechanical[31] and thermal properties[32] and low cost make EDA-NCNT a potential material to replace platinum-based catalysts in fuel cell cathodes. Through the comparison of EDA-NCNT and Py-NCNT, the effect of nitrogen precursors on nitrogen content and the fundamental role of nitrogen content in the ORR activity were demonstrated. As a conclusion, EDA-NCNT containing high nitrogen content is a promising material for the ORR catalysis in FCs.

Acknowledgment. This work was financially supported by the Natural Sciences and Engineering Research Council of Canada (NSERC) and the University of Waterloo.

References and Notes

(1) Zhang, L.; Zhang, J. J.; Wilkinson, D. P.; Wang, H. J. *J. Power Sources* **2006**, *156*, 171.
(2) Limjeerajarus, N.; Yanagimoto, T.; Yamamoto, T.; Ohashi, H.; Ito, T.; Yamaguchi, T. *J. Chem. Eng. Jpn.* **2009**, *42*, 39.
(3) Arico, A. S.; Bruce, P.; Scrosati, B.; Tarascon, J. M.; Van Schalkwijk, W. *Nat. Mater.* **2005**, *4*, 366.
(4) Bauen, A.; Hart, D. *J. Power Sources* **2000**, *86*, 482.
(5) Garcia, B. L.; Sethuraman, V. A.; Weidner, J. W.; White, R. E.; Dougal, R. *J. Fuel Cell Sci. Technol.* **2004**, *1*, 43.
(6) Bashyam, R.; Zelenay, P. *Nature* **2006**, *443*, 63.
(7) Feng, Y. J.; He, T.; Alonso-Vante, N. *Chem. Mater.* **2008**, *20*, 26.
(8) Liu, D.; Yang, J.; Gosztola, D. J. *ECS Trans.* **2007**, *5*, 147.
(9) Wang, C.; Waje, M.; Wang, X.; Tang, J. M.; Haddon, R. C.; Yan, Y. S. *Nano Lett* **2004**, *4*, 345.
(10) Shao, Y. Y.; Liu, J.; Wang, Y.; Lin, Y. H. *J. Mater. Chem.* **2009**, *19*, 46.
(11) Shao, Y. Y.; Sui, J. H.; Yin, G. P.; Gao, Y. Z. *Appl. Catal., B* **2008**, *79*, 89.
(12) Maldonado, S.; Stevenson, K. J. *J. Phys. Chem. B* **2005**, *109*, 4707.
(13) Matter, P. H.; Wang, E.; Arias, M.; Biddinger, E. J.; Ozkan, U. S. *J. Mol. Catal. A: Chem.* **2007**, *264*, 73.
(14) Matter, P. H.; Wang, E.; Arias, M.; Biddinger, E. J.; Ozkan, U. S. *J. Phys. Chem. B* **2006**, *110*, 18374.
(15) Gong, K. P.; Du, F.; Xia, Z. H.; Durstock, M.; Dai, L. M. *Science* **2009**, *323*, 760.
(16) Lefevre, M.; Dodelet, J. P.; Bertrand, P. *J. Phys. Chem. B* **2002**, *106*, 8705.
(17) Yang, J. B.; Liu, D. J.; Kariuki, N. N.; Chen, L. X. *Chem. Commun.* **2008**, 329.
(18) Maldonado, S.; Stevenson, K. J. *J. Phys. Chem. B* **2004**, *108*, 11375.
(19) Terrones, M.; Terrones, H.; Grobert, N.; Hsu, W. K.; Zhu, Y. Q.; Hare, J. P.; Kroto, H. W.; Walton, D. R. M.; Kohler-Redlich, P.; Ruhle, M.; Zhang, J. P.; Cheetham, A. K. *Appl. Phys. Lett.* **1999**, *75*, 3932.
(20) Terrones, M.; Redlich, P.; Grobert, N.; Trasobares, S.; Hsu, W. K.; Terrones, H.; Zhu, Y. Q.; Hare, J. P.; Reeves, C. L.; Cheetham, A. K.; Ruhle, M.; Kroto, H. W.; Walton, D. R. M. *Adv. Mater.* **1999**, *11*, 655.
(21) Sumpter, B. G.; Meunier, V.; Romo-Herrera, J. M.; Cruz-Silva, E.; Cullen, D. A.; Terrones, H.; Smith, D. J.; Terrones, M. *ACS Nano* **2007**, *1*, 369.
(22) Jang, J. W.; Lee, C. E.; Lyu, S. C.; Lee, T. J.; Lee, C. J. *Appl. Phys. Lett.* **2004**, *84*, 2877.
(23) Sumpter, B. G.; Huang, J. S.; Meunier, V.; Romo-Herrera, J. M.; Cruz-Silva, E.; Terrones, H.; Terrones, M. *Int. J. Quantum Chem.* **2009**, *109*, 97.
(24) Elezovi, N.; Babi, B.; VRA AR, L.; Krstaji, N. *J. Serb. Chem. Soc* **2007**, *72*, 699.
(25) Solorza-Feria, O.; Ram rez-Raya, S.; Rivera-Noriega, R.; Ordoz-Regil, E.; Fernandez-Valverde, S. *Thin Solid Films* **1997**, *311*, 164.
(26) Liu, J.; Czerw, R.; Carroll, D. L. *J. Mater. Res.* **2005**, *20*, 538.
(27) Matter, P. H.; Zhang, L.; Ozkan, U. S. *J. Catal.* **2006**, *239*, 83.
(28) Maldonado, S.; Morin, S.; Stevenson, K. J. *Carbon* **2006**, *44*, 1429.
(29) Ghosh, K.; Kumar, M.; Maruyama, T.; Ando, Y. *Carbon* **2009**, *47*, 1565.
(30) Yang, Q. H.; Hou, P. X.; Unno, M.; Yamauchi, S.; Saito, R.; Kyotani, T. *Nano Lett.* **2005**, *5*, 2465.
(31) Wong, E. W.; Sheehan, P. E.; Lieber, C. M. *Science* **1997**, *277*, 1971.
(32) Berber, S.; Kwon, Y. K.; Tomanek, D. *Phys. Rev. Lett.* **2000**, *84*, 4613.

JP908067V